

# Improving on Hydropower Mitigation Success by Refining Predictions of Grain Motion

Heidi J. Smith

December 31, 2014

## Project Summary

My research aims to improve on grain motion predictions in rivers by including the effects of turbulence in a model based on inputting values of easily measureable parameters (i.e. slope, depth, velocity, and grain size distribution). This will be a valuable tool for hydropower projects to improve the prediction of grain motion in mitigation sites, as well as improving on predictions of reservoir fill rates.

# Chapter 1

## An Investigation into the Turbulence Parameter Responsible for the Onset of Grain Motion

Heidi J. Smith, Elowyn M. Yager, and Ralph S. Budwig

### Abstract

The use of traditional bedload transport equations result in substantial errors in streams where fluxes are over-predicted by orders of magnitude. These equations often use excess shear stress, which is a function of the difference between the mean applied and critical shear stresses. However, in steep streams wide distributions of both applied and critical stresses exist, which result in a spatial and temporal variability of the onset of motion. Therefore, the use of mean stresses does not accurately represent motion for these systems. Turbulence is responsible for the wide variability of applied shear stresses, however we currently do not understand the mechanics of how turbulence causes motion. We conducted a set of flume experiments of grain motion that measures the turbulence parameters of velocities, forces and pressures on a mobile test grain. By analyzing velocity, pressure and force datasets, we explored the turbulence parameter(s) responsible for motion. We measured (1) velocities using 3D particle imaging velocimetry along a stream-wise transect over a grain, (2) spatial distributions of pressures using seven sensors embedded inside the mobile grain, and (3) forces on the grain using three load cells. The critical shear stress of the mobile grain is held relatively constant through all experiments by fixing its pocket geometry, whereas mean slope, water depth and velocity are varied between experiments. Using these data, we identified the responsible parameter by quantifying which is/are the most statistically significant at motion. Our results suggest that the integrative effect of velocity in a profile along the upstream side of a grain may best correspond to its motion. We observed that particle motion corresponds with (1) drag force, (2) a large portion of the grain being subjected to statistically high velocities, (3) a large value of summed statistically high values of velocity, (4) a high mean value of velocity across the entire front surface of the grain, and (5) a single high value of velocity. These results suggest that turbulence excursions of a certain size and magnitude must occur over enough of the grain for motion to occur. This also suggests that a single location upstream of a grain does not completely describe the turbulence that causes motion. Of the turbulence parameters tested using the pressure dataset, drag force corresponds best to sediment motion. Finally, the predictive ability of the tested turbulence parameters did not have a clear trend with channel slope.

# 1 Introduction

Accurately predicting the onset of grain motion in rivers is a component to predict sediment fluxes, which is important for management efforts such as restoration, risk prevention, stabilization of banks and also predicting fill rates of reservoirs. Current sediment transport equations overpredict sediment loads by a few orders of magnitude (Gomez and Church, 1989), which is likely due to problems related to predicting the onset of sediment motion. First, to predict flux, excess shear stress is often used, which is the shear stress that exceeds the critical value at the onset of grain motion. Near this threshold of motion, bedload fluxes are non-linearly related to the changes in shear stress, so the use of excess shear stress results in large changes of fluxes with small increases in shear stress. Therefore, small errors in the critical shear stress results in large errors in sediment fluxes. Also, the approach of using an average shear stress to predict sediment fluxes is fundamentally flawed because sediment motion is highly dependent on the local stresses caused by near-bed turbulence, which varies temporally and spatially, and a single average shear stress cannot account for this. Studies have attempted to include turbulence to improve sediment flux predictions, by assuming a range of applied shear stresses (e.g. McEwan et al., 2004), but this approach still does not directly address local forces at the grain scale, where the problem lies. In this paper, we begin to address this issue by identifying which turbulence parameter is responsible for grain motion, which may be used as the foundation for a new model that predicts the onset of sediment motion based on sediment-flow motion mechanics.

The effect of turbulence on sediment motion is important because as turbulence develops, the ability of a given average shear stress near the motion threshold changes (Nelson et al., 1995). First, Clifford et al. (1991) observed that turbulence events (sweeps, bursts, outward and

inward interactions) are correlated with motion. Sweeps (positive  $u'$  and negative  $w'$ ), increased average shear stress, and were found to cause the most sediment motion due to the high probability of occurrence while outward interactions, (positive  $u'$  and positive  $w'$ ) decreased average shear stress, and caused equal motion per equivalent magnitude, but less sediment motion overall because they occurred less frequently (Nelson et al., 1995). In a developing boundary layer the percentage of velocity excursions changes, and thus, for a given average shear stress, more or less sediment motion occurs (Nelson et al., 1995). Though it is known that turbulence alters sediment motion thresholds, it is still unknown which turbulence parameter or combination of parameters is responsible for motion (Kalinske, 1943; Nelson et al., 1995; Papanicolaou et al., 2001; Schmeeckle et al., 2007; Coleman and Nikora, 2008).

Numerical and flume experiments have focused on motion-causing mechanisms around a single grain. Turbulence impulse, which is a combination of drag force and its duration, is coupled with grain motion (Diplas et al., 2008). Near-bed pressure fluctuations, another property of turbulence, cause distributions of lift and drag forces on grains. Additionally, permeability of bed material to water flow also affects the amount of lift on a grain by changing the vertical gradient of pressure (Hofland, 2005; Vollmer et al., 2002; Vollmer, 2005; Packman et al., 2004). Exactly how pressures vary around a grain which causes its motion remains to be known.

Finally, the forces applied to a grain due to turbulence have been measured directly with the use of a load cell by Schmeeckle et al. (2007). In this study, they measured nominal lift and drag forces upon a grain when varying protrusion, or the height at which the grain extended into the flow, and simultaneously measured near-grain upstream velocities at a point. They concluded that the drag force correlates with stream-wise velocity. Finally, as a grain's

protrusion increases, the drag force and standard deviation of these forces increases, while the lift force decreases and standard deviations increases. This suggests that with increased protrusion, drag force becomes more important, and lift becomes less important for motion.

In this paper, we aim to improve the understanding of turbulence-grain interactions by isolating turbulence parameters most responsible for grain motion around a test grain during its motion. To accomplish this we conducted a set of flume experiments in which we measured velocity, pressure and force fluctuations through a grain’s motion at varying reach-average slopes, and consequently at varying depths and velocities. By measuring the distribution of these turbulence properties, we aim to isolate the characteristic of turbulence and the local mechanism that most often causes grain motion.

## 2 Methods

### 2.1 Data Collection

#### *Measuring local turbulence*

We measured local turbulence around a single instrumented mobile test grain (Figure 1) before and through its motion for a range of reach-averaged hydraulic parameters that exist in natural rivers. The test grain was constructed using a rigid, hollow, plastic sphere that was 50 mm in diameter, which was weighted with lead, so that its density was that of granite (2.675 g/cm<sup>3</sup>). Also, upon the surface of the test grain, we glued a layer of

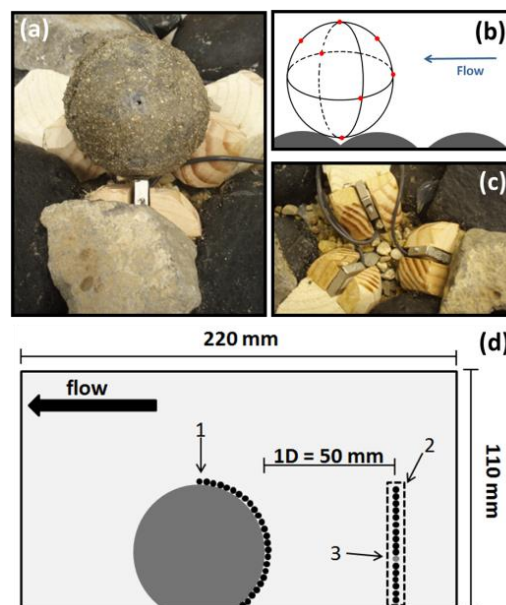


**Figure 1** The instrumented mobile test grain (a) and the methods used to measure turbulence parameters: (b) Pressure- transducer locations are indicated with red dots, (c) Force- load cells were positioned underneath the grain, and (d) Velocity- vector field was analyzed in the 3 indicated locations: 1.) upstream side of the grain, 2.) vertical profile 1 grain diameter upstream of the test grain, and 3.) one point located one diameter upstream of the test grain, and half of a diameter high.

sand to mimic the roughness of a rock. We measured the following three properties of turbulence around the grain before and during its motion (Figure 1): (a) instantaneous pressures around the test grain using 7 internally-placed micro pressure sensors, with ports exposed to the flow, (b) instantaneous velocities in a stream-wise transect of flow around the grain, and (c) instantaneous forces using 3 load cells arranged in a triangular configuration on which we placed the test grain. Motion of our test grain was defined as when it completely rolled off of the downstream load cells. For all moments of motion, the grain rolled in this streamwise direction. The grain did not travel far because it remained tethered to the plate with wires that the pressure sensors were attached to, that exited the test grain on its downstream, lower side. These wires were selected based on their narrow and flexible quality to lower their effect on the local flow and also the motion of the test grain. The pressure and force datasets were synchronized and were collected at 5000 hz, and the velocity dataset was collected at 17 hz.

#### *Measuring pressures around the test grain*

To measure pressures around the test grain, we positioned the pressures port locations around the grain to facilitate calculations of drag and lift forces due to pressure differentials around the grain (Figure 1b). These locations were (1) upstream-most, (2) midpoint between downstream-most and top (3) top, (4) bottom, (5) midway between the upstream-most and top sensor, (6) left, and (7) right. Before each experimental run, the pressure ports were exhumed of air by using a syringe to force out all bubbles. This insured that we were measuring water pressure and not air pressure.

### *Measuring velocities around the test grain*

Particle Imaging Velocimetry (PIV) was used to measure 3D velocities around the test grain in a streamwise-oriented transect. The program DaVis developed by the company LaVision was used to collect and process the velocity dataset. Our PIV

configuration used two cameras, which were both focused on the test grain and placed on one side of the flume, such that one camera was upstream and one camera was downstream of the test grain (Figure 2). The cameras were calibrated for the location of the test grain, which was held constant throughout all experiments. Next, a thin laser argon sheet illuminated neutrally buoyant particles in the flow and were recorded by the cameras as an image per laser pulse. From each image, a cross-correlation analysis of particles was used to create a velocity vector for each interrogation region by using the average velocity and direction of all particles captured within that region. This process was the basis for creating a vector field, which was 220 mm wide in the streamwise direction by 110 mm in the vertical direction around the test grain. For our analysis, we used all components of velocities: streamwise ( $u$ ), vertical ( $w$ ), and lateral ( $v$ ) velocities. To test the turbulence parameters using the velocity dataset, we treated the 3 components of velocity separately, to explore the effects of each component upon motion independently.

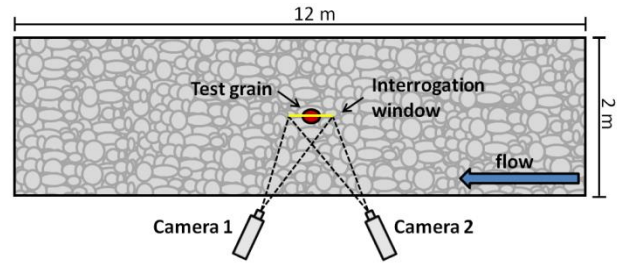


Figure 2 Plane view of the PIV flume configuration. The cameras were angled to measure velocities in 3 dimensions around the test grain. The streamwise length interrogation window is also depicted (yellow line).

### *Fixing bed resistance applied to the test grain*

We placed the test grain upon three load cells that could detect the grain's movements. The load cells were fixed upon a heavy metal plate upon which gravels were glued, to ensure the local bed configuration was held constant throughout all experiments. We selected the most simple configuration for the load cells, with their contact points with the test grain being equidistant from each other (3 cm) and at an equal angle ( $35.5^\circ$ ) from horizontal (Figure 2b). We positioned this load cell configuration so that one load cell was positioned facing upstream, while the other two were facing downstream on the left and right of the test grain. For all runs, we placed the test grain in the same orientation upon these fixed load cells to ensure the resisting force of the underlying grain upon the test grain remained constant. The friction angle is a proxy for the stability of a grain upon a bed, and is the angle that if the channel slope was increased to, the grain would rotate from its pocket due to the weight of the grain. We used friction angle to calculate critical drag based, used in the impulse parameter (section 3.1.2). We measured our configuration's friction angle ( $35.5^\circ$ ) by tilting the plate upon which the grain arrangement was placed upon multiple times, until the grain rolled from its pocket (Kirchner et al., 1990), and took the average of these values. The configuration of the test grain in its pocket remained constant throughout all experiments, so the friction angle also remained constant. The protrusion of our test grain, or the vertical distance of the test grain that extended into the flow beyond the immediate grain upstream, was 30 mm and remained constant throughout our experiments. This protrusion was relatively high, which we selected in order to measure turbulence at the initial motion of our bed when the test grain moved. Additionally, protruding grains would be the first to move in natural rivers as well.

### *Identifying grain motion*

We defined grain motion as the moment the grain started rotation from its pocket prior to its complete rotation. This moment was identified within the pressure dataset when the synchronized upstream load cell signal finally fell in magnitude, marking when the test grain separated from it. The moment of motion was identified within the PIV dataset when the photographs, which were collected at the same moments as the vector fields, showed when the test grain first began rotation.

### *Measuring reach-averaged hydraulic properties*

We measured turbulence around our test grain for a range of channel slopes to explore how the identified responsible turbulence parameter changed with slope and other reach-averaged hydraulic parameters. The laboratory flume used

to conduct these experiments can tilt through a large range of slopes (0.6% -10%), and its large size (20 meters long, 2 meters wide and 1.5 meters high) reduces the potential for error when scaling up to larger rivers. For this set of experiments, we used slopes between 0.63 -

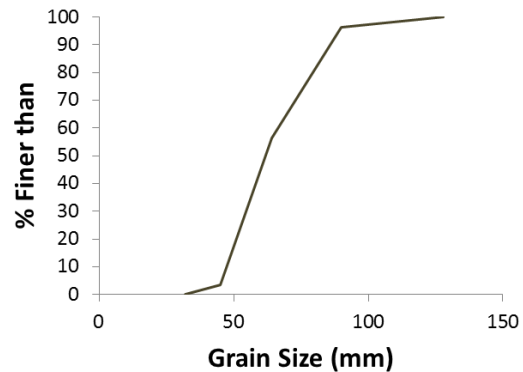


Figure 3 Grain size distribution of the bed material.

2.6%, and our test section was 20 m long, positioned in the center of the flume which was lined with sediment with a D50 of 70 mm. The bed's grain size distribution (Figure 3) was large enough so the bed rarely moved in the flow conditions that caused the test grain to move; therefore, the bed was largely immobile. To decrease the upstream boundary effects, we used a flow straightener. Additionally, at the downstream end of the flume, an adjustable gate was used to establish uniform flow over the entire test section. To decrease sidewall boundary effects, the grain was positioned at the midpoint between the flume sidewalls and halfway between the

upstream and downstream boundary of the test section. The change in slope will change the downstream component of force on the test grain.

We selected 5 slopes with the widest range that would not mobilize the bed under flow conditions in which the test grain was mobile. For each slope, we slowly and incrementally increased the discharge until our test grain moved. By increasing the discharge in this manner, we monitored grain motion due to turbulence rather than motion due to a stream-wise acceleration of flow caused by non-uniform flow. For each slope, we captured from 4-7 grain motions.

Immediately following each grain motion, we quantified the reach-averaged hydraulic conditions, to develop a relationship between the local turbulence around the test grain and the average flow conditions. First, we calculated the average flow depth from measurements of water depth at random distances along the length of the flume that incorporated depth fluctuations due to surface waves. Next, to quantify reach-averaged velocities per experimental run, we used the continuity equation  $U = Q/(w \cdot h)$  ( $U$  = average velocity,  $Q$  = average discharge,  $w$  = channel width, and  $h$  = average depth) with the known inputs of discharge and the measured cross sectional area of the flume. The cross-sectional area of the flume was calculated using reach-averaged depths, and the width of the flume ( $w \cdot h$ ). To calculate the average shear stress for each run, when the grain moved we used the equation  $\tau = \rho g h S$ , where  $\rho$  is the density of water,  $g$  is the acceleration due to gravity,  $h$  is the average depth of the flume test section and  $S$  is the slope of the flume. Discharge was automatically measured once every 5 seconds, with an error of 0.5% using an UltraMag electromagnetic flow meter, which uses high density magnetic coils to create an electromagnetic field inside a pipe, that then voltage created by the flowing water is measured with electrodes, and is finally converted to a flow rate.

### 3 Data Analysis

#### Velocity dataset- selecting locations to analyze

From each vector field, we extracted velocity data in three zones (Figure 1d) relative to the grain. In zone 1, we extracted vectors immediately upstream and adjacent to the test grain. To avoid selecting a location with fluid velocities which had slowed too much due to the test grain, but close enough to be the best correlated with motion, we chose grid cells that were located just beyond 2 mm in either the horizontal or vertical direction from the grain's surface. In zone 2, we extracted a profile of flow, located one diameter upstream of the test grain that extended from the sediment bed to the height of the test grain. We chose this height, rather than the entire flow depth that varied by slope, so all runs could be compared. Finally, zone 3 was selected at one point, one diameter upstream of the test grain to compare with recent studies that have used this location (e.g. Diplas 2008, Schmeeckle 2007).

#### Velocity dataset- defining motion causing flow

Our main analysis goal was to explore which turbulence parameter best corresponded to our test grain moving. Therefore, we used each location's velocity time series to test if various turbulence parameters were statistically higher during motion-causing flow (MCF), compared to flow that the grain remained stable, or stable grain flow (SGF). To define the number of frames that

measured MCF for each zone, we first identified when the grain started rotation within the video

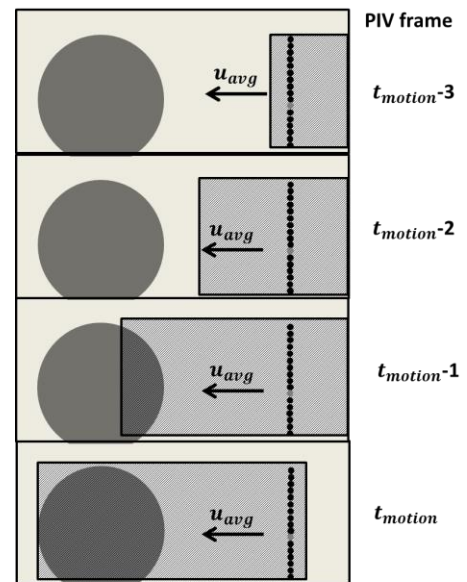


Figure 4 Schematic illustrating which PIV frames captured Motion-Causing Flow (MCF)- this example run shows frame selection prior to grain rotation for zone 3. The assumed speed of the shaded parcel of fluid is based on the time-averaged  $u$  component of velocity at zone 3 for each run.

frames collected by DaVis. We then assumed that frames prior to the grain beginning rotation also included MCF, because all zones where velocity vectors were extracted were upstream relative to the grain. We assumed that the MCF may have already passed zones 1-3 prior to the beginning of rotation. Thus, we needed to find all frames prior to the moment of rotation (Figure 4). To do this, we first calculated the time-averaged u component of velocity for the fluid that passed location 3. Based on the distances between each zone to the downstream side of the test grain (50 mm for zone 1 and 100mm for zones 2 and 3), we calculated the average travel time for a parcel of fluid to travel this distance. With this time, we calculated the number of frames prior to grain rotation which may have included MCF. The streamwise component of velocity at zone three increased as we increased slope between runs, therefore the number of frames that bracketed motion also changed.

#### *Velocity dataset- turbulence parameters tested*

##### Parameter1: Sum of statistically high velocities

With this parameter, our aim was to test the importance of having a combination of high magnitude velocities over a large portion of the grain. To extract only the largest turbulent fluctuations, we included only the high velocities within each grid cell through time. To extract these high velocities from the dataset, we considered each grid cell within each zone as a separate distribution of velocities. Zone one had 25 grid cells and zones two had 17 grid cells. For each grid cell, we converted the distribution of velocities (u, v, and w) into z scores. A z score is a standardized number, whose value is the number of standard deviations above or below the mean (e.g. -2 and 2 are equal to two standard deviations below and above the mean respectively). Therefore, this conversion allowed us to identify statistically high velocities for

each grid cell. Also, because velocities decrease as they approach the bed, converting to z scores allowed us to compare different grid cells with one another. This dataset of z scores became the basis for this turbulence parameter, as well as the next three parameters described below.

For each run, a certain number of frames were considered as part of Stable Grain Flow (SGF) and as well as part of Motion Causing Flow (MCF). For each of these frames, we summed the magnitudes of statistically high standardized velocities for each zone, which resulted in one value of summed magnitudes per frame, per zone. If a higher value of summed magnitudes occurred within the MCF frames, we considered that for this run, summed magnitude of statistically high standardized velocities may have caused this grain motion. If the opposite occurred, that the summed value before motion was greater than during motion, then this parameter on this run may have not cause motion.

#### Parameter 2: Area of Grain Subjected to Statistically High Velocities

Our goal was to investigate if grain motion corresponded to a large portion of the test grain being subjected to statistically high velocities. We hypothesized that a parcel of fluid that causes motion would encompass a large portion of the test grain. This parameter focus only on the portion of the grain being subjected to high velocities without considering the standardized magnitudes of high velocities as performed in parameter one. For parameter two, we used the dataset of statistically high standardized velocities described in parameter one to calculate the number of grid cells within each velocity zone with statistically high velocities. To test the dependence of grain motion on this parameter, for each run, we divided the total frames into those that included SGF and those that included MCF. For each frame, both zones 1 and 2 had an associated number of grid cells with statistically high velocities. For each zone, if the

maximum value of this parameter occurred during MCF, then during this run, the portion of the grain subjected to statistically high velocities was considered to cause motion.

### Parameter 3: Maximum standardized velocities

Within this parameter, we calculated the maximum standardized velocity (u, w and z separately) per time step, for each zone. By testing this parameter, we aimed to find if the peak velocity alone corresponded with grain motion. Here, we hypothesized that a high velocity excursion may be important for motion.

### Parameter 4: Mean of standardized velocities

We calculated the mean of all of the statistically high z scores in each zone for each time step during SGF and compared it to the mean during MGF. This parameter aimed to explore if the mean of all statistically high velocities determined motion. With this parameter, we explored if the grain motion was dependent on the average of high velocities.

### Parameter 5: Drag Force

To compute drag force per time step, we used the equation:

$$F_D = \frac{1}{2} C_d * \rho * A * u^2 ,$$

where  $C_d$  is the drag coefficient for a natural gravel (0.91) (Schmeeckle et al., 2007), which we selected based on our test grain having a roughened surface similar to a natural grain,  $\rho$  is the density of water (1000 kg/m<sup>3</sup>),  $A$  is the cross-sectional area of the grain perpendicular to the flow. For the velocity profiles in zones 1 and 2, we integrated the equation for a sphere into horizontal slices (Yager et al., 2007), and used the velocity of the respective pixel at each slice to calculate the drag force for that slice. Therefore, for each horizontal slice, we computed a drag force, and used the appropriate cross-sectional area of the test grain for that slice and the  $u$

component of velocity at each associated grid cell. Then, we summed the drag forces applied to all slices to calculate a total drag force on the test grain for each frame. For the point dataset of zone 3, we used the entire cross-sectional area and applied the changing values of  $u$  through time to calculate the drag force.

#### Parameter 6: Impulse

We tested the impulse parameter based on Diplas et al.'s (2008) definition of an impulse event and is calculated with the equation:

$$\text{Impulse event} = \int_{t_1}^{t_2} F * d(t),$$

where  $F$  is the average of drag force that exceeds the critical force from time from  $t_1$  to when the drag force falls below the critical drag value at time  $t_2$ , and  $d(t)$  is the duration the critical drag is exceeded. We calculated the critical drag force by using the equation that calculates the resisting force of the underlying bed upon a grain established by Wiberg and Smith (1990):

$$F_R = F_N * \tan\phi,$$

where  $F_R$  is the resisting force of the bed material on the test grain,  $F_N$  is the weight of the test grain minus buoyancy, and  $\phi$  is the grain's friction angle. Following Diplas et al.'s (2008) methods, we calculated the impulse that occurred during grain motion, and compared the magnitude of this impulse event to all impulse events that occurred during SGF.

*Pressure dataset- turbulence parameters tested*

#### Parameter 5: Drag Force

To compute drag forces using the pressure data, for each time step, we subtracted the upstream-most pressure to the downstream pressure sensor to calculate a differential pressure. Then, we multiplied this differential pressure by the cross-sectional area of the test grain.

Parameter 6: Impulse

To compute impulses for each run, we used the drag force time series that was calculated using the pressure data. To compute impulses, we computed all other steps in the same way described using the velocity data.

## 4 Results

*Reach-average hydraulic parameters at grain motion*

At grain motion, the calculated reach-averaged hydraulic parameters show a trend with slope (Figure 5). The average velocity decreases with slope, the average depth decreases with slope and the average critical shear stress increases with slope. To compare with the reach-averaged velocity, we also graphed the near-bed streamwise time-averaged component of velocity at zone 3. The average near-bed streamwise velocity trend follows the reach-averaged velocity by decreasing with slope until 1.0% slope, when the near-bed velocity increases. Thus, for the steeper slopes, at the threshold of sediment motion, the reach-averaged and near-bed streamwise velocity have an opposite relationship with slope.

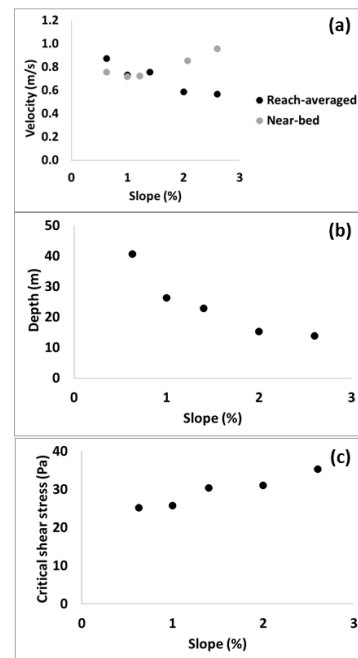


Figure 5 Reach-averaged hydraulic parameters at grain motion, between each channel slope. For comparison, an average near-bed time-averaged u component of velocity for each slope was calculated using zone 3 datasets.

Testing turbulence parameters using velocity dataset

Testing parameters using streamwise velocities (u)

Of the six turbulence parameters we tested using our velocity dataset (Table 1, Parameters 1-6), three could be tested using the zone 3. With the exception of impulse, the zone immediately upstream and adjacent to the test grain, had the highest number of successful

Table 1 Turbulence parameters tested

Parameter	Description
1	Sum of statistically high velocities
2	Portion of profile with statistically high velocities
3	Maximum velocity
4	Mean of statistically high velocities
5	Drag
6	Impulse

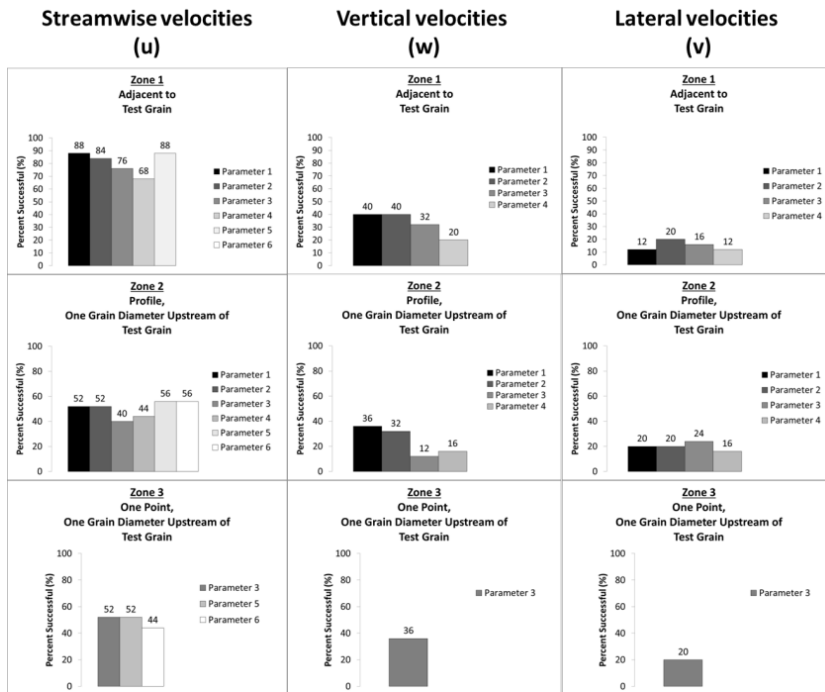


Figure 6 Percentages of Successful Runs per Parameter in the three zones for 3 components of velocity, streamwise (u), vertical (w), and lateral (v). Six turbulence parameters were tested using our velocity dataset: 1.Sum of statistically high velocities, 2. Portion of profile with statistically high velocities, 3. Maximum velocity, 4. Mean of statistically high velocities, 5. Drag Force, and 6. Impulse. The parameters for each bar graph were the parameters tested for that velocity component/velocity zone combination. If a parameter is listed on a bar graph, but without a bar, this parameter was tested, but the result was 0% success.

runs for all parameters (Figure 6). The other two zones, both located one grain diameter upstream from the test grain, resulted in similar percentages of successful runs to one another, approximately 50%. These results suggest the velocities immediately upstream and adjacent to the test grain had the most predictive velocity vectors, and the drag force parameter number 6, had the best rate of

success. Parameters 5 and 6 could only be tested with the streamwise component of velocity because the u component is the basis for drag and impulse calculations.

*Testing parameters using vertical (w) and lateral (v) velocities*

Overall, vertical velocities performed more poorly than streamwise velocities, but better than lateral velocities (Figure 6). The parameters' success of vertical velocities followed the pattern of success of the streamwise component (e.g. parameter performed the best, then parameter 2 and so on, in both components. The success rates of various parameters of the lateral velocities did not follow the pattern of streamwise and vertical.

*Success rate and channel slope*

We were interested in observing if each parameter performed differently between channel slopes. With the parameters that used streamwise component of velocity, we found that there is not a clear trend between slopes (Figure 7).

*Testing turbulence parameters using pressure dataset*

Using our pressure data, we found that the magnitude of drag force performed better than impulse(Figure 8).

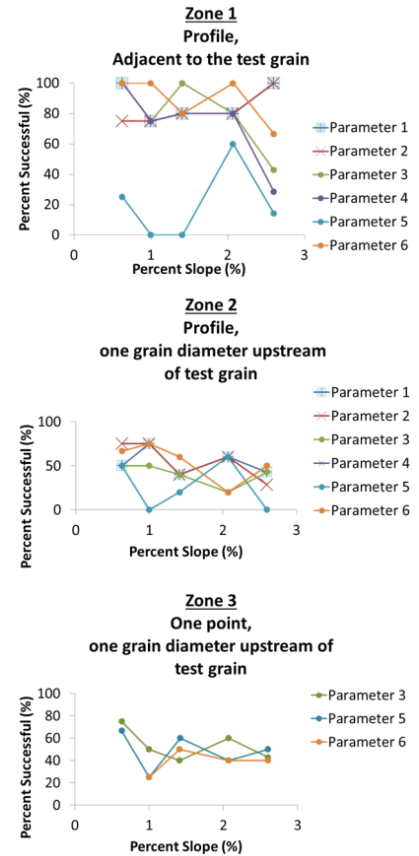


Figure 7 Success rate for turbulence parameters using streamwise component of velocity for three velocity extraction zones.

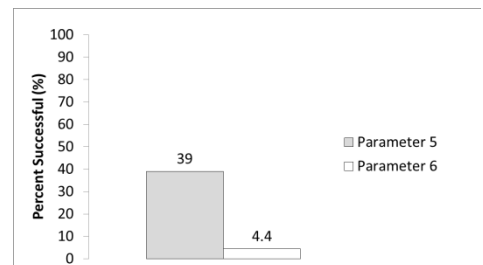


Figure 8 Percent success for the turbulence parameters using the pressure dataset

## 5 Conclusions

1. Reach-averaged velocity has an opposite trend with slope than the near-bed time-averaged  $u$  component of velocity.
2. Overall, the high number of successful runs for parameters in the zone immediately upstream and adjacent to the grain suggests that monitoring velocity in a profile and in this location, rather than one diameter upstream, may be important for predicting motion.
3. The drag force parameter best predicts motion when tested in the zone immediately adjacent and upstream of our test grain.
4. The streamwise and vertical components of velocities have the highest predictive ability.

## References Cited

- Clifford, N. J., McClatchey, J., French, J. R. , 1991. Measurements of turbulence in the benthic boundary layer over a gravel bed and comparison between acoustic measurements and predictions of the bedload transport of marine gravels. *Sedimentology*, 38, 161–171.
- Diplas, P., Dancey, C. L., Celik, A. O., Valyrakis, M., Greer, K., and Akar, T., 2008. The role of impulse on the initiation of particle movement under turbulent flow conditions. *Science*. 322, 717-720.
- Coleman, S. E., Nikora, V. I., 2008. A unifying framework for particle entrainment. *Water Resources Research*, 44. W04415, DOI: 10.1029/2007WR006363.
- Gomez, B., & Church, M. (1989). An assessment of bed load sediment transport formulae for gravel bed rivers. *Water Resources Research*, 25(6), 1161-1186.
- Hofland, B., Battjes, J. A., Booij, R., 2005. Measurement of fluctuating pressures on coarse bed material. *J. Hydraul. Eng.* 131, 770– 781.
- Kalinske, A. A., 1943. Turbulence and the transport of sand and silt by wind. *Annals N. Y. Acad. Sci.* 44: 41-54.
- Vollmer, S., Ramos, F., Daebel, H., Kühn, G., 2002. Micro-scale exchange processes between surface and subsurface water. *J. Hydrol.* 269 (1), 3–10.
- Vollmer, S., 2005, Einfluß der Oberflächenströmung auf die permeable Gewässersohle, *Mitt. Inst. Wasserwirt. Kulturtech.* 231, Univ. Karlsruhe, Karlsruhe, Germany.
- McEwan, I., Sørensen, M., Heald, J., Tait, S., Cunningham, G., Goring, D., Willets, B. 2004. Probabilistic modeling of bed-load composition. *J. Hydraul. Engng.* 130 (2), 129-139
- Nelson, J. M., Shreve, R. L., McLean, S. R., Drake, T. G., 1995. Role of near-bed turbulence structure in bed-load transport and bed form mechanics. *Water Resources Res.* 31(8), 2071-2086.
- Packman, A. I., Salehin, M., and Zaramella, M., 2004. Hyporheic exchange with gravel beds: basic hydrodynamic interactions and bedform-induced advective flows. *Journal of Hydraulic Engineering* 130, pp. 647–656.
- Papanicolaou, A., Diplas, P., Dancey, C., Balakrishnan, M., 2001. Surface roughness effects in near-bed turbulence: Implications to sediment entrainment. *J. Eng. Mech.* 127 (3), 211–218.
- Schmeeckle, M. W., Nelson, J. M., Shreve, R. L., 2007. Forces on stationary particles in near-bed turbulent flows. *J. Geophys. Res.* 112, F02003, doi:10.1029/2006JF000536.
- Yager, E.M., Kirchner, J.W., Dietrich, W.E., 2007. Calculating bed load transport in steep boulder bed channels. *Water Resources Research* 43: W07418. DOI: 10.1029/2006WR005432

Upon graduation in May of 2015, the following chapters will also be completed and submitted:

Chapter 2

Development of a Grain Motion Predictive Model, that Builds Upon the Turbulence Parameter Responsible for Grain Motion

Chapter 3

Testing the Gain Motion Predictive Model in the Field

Acknowledgement:

The information, data, or work presented herein was funded in part by the Office of Energy Efficiency and Renewable Energy (EERE), U.S. Department of Energy, under Award Number DE-EE0002668 and the Hydro Research Foundation.

Disclaimer:

The information, data or work presented herein was funded in part by an agency of the United States Government. Neither the United States Government nor any agency thereof, nor any of their employees, makes and warranty, express or implied, or assumes and legal liability or responsibility for the accuracy, completeness, or usefulness of any information, apparatus, product, or process disclosed, or represents that its use would not infringe privately owned rights. Reference herein to any specific commercial product, process, or service by trade name, trademark, manufacturer, or otherwise does not necessarily constitute or imply its endorsement, recommendation or favoring by the United States Government or any agency thereof. The views and opinions of authors expressed herein do not necessarily state or reflect those of the United States Government or any agency thereof.